Journal of Magnetism and Magnetic Materials 563 (2022) 169939

Contents lists available at ScienceDirect

Journal of Magnetism and Magnetic Materials

journal homepage: www.elsevier.com/locate/jmmm

A novel positioning method for magnetic spiral-type capsule endoscope using an adaptive LMS algorithm

Bo Ye [a], Guo Fang [a], Jinping Hu [a], Hao Wang [a], Yingbing Fu [a], Shicong Zhang [a], Amit Krishna Dwivedi [b,*]

[a] *School of Computer Science and Information Engineering, Hubei University, Wuhan 430062, China*
[b] *Department of Engineering, Manchester Metropolitan University, Manchester M15 6BH, United Kingdom*

ARTICLE INFO

Keywords:
Wireless capsule endoscope
Magnetic sensor array
Magnetic positioning
Active control
Adaptive LMS algorithm

ABSTRACT

In this paper, a novel positioning method for the wireless capsule endoscope (WCE) is proposed. An up-down symmetric array of magnetic sensors is used to detect magnetic signals from an external permanent magnet (EPM) for active control and mixed magnetic signals (the EPM and the WCE), and the adaptive least mean squares (LMS) algorithm is applied. Firstly, the number of iterations is determined by comparing the cancellation effect of input signals of different lengths. Subsequently, to separate the WCE's magnetic signals from the mixed magnetic signals, the data obtained from the magnetic sensor arrays are processed in weighted iterations. The method has been applied to the actual experimental platform. From the experimental results achieved in this work, the average relative errors of the WCE's triaxial signals were found to be 2.04 %, 2.20 %, and 1.47 % respectively. Achieved results demonstrate the feasibility and rationality of the positioning method discussed in this work. Moreover, the method can solve the problem of strong magnetic interference when the EPM provides active control to the WCE. It plays an essential role in driving the realization of closed-loop control of the WCE.

1. Introduction

Due to the accelerating pace of life in today's culture, many people have developed unhealthy eating and sleeping habits. In addition, environmental issues such as air pollution, are making a huge impact on human health, reducing the quality of life on a daily basis. These issues have also limited access to a sufficient amount of safe and nutritious food for humans resulting in several foodborne diseases. Amongst others, gastroenteritis is one of the most common infections with a significant increase in the number of patients being hospitalized around the globe [1,2]. The traditional method used for the examination of gastroenteritis, such as the wireline gastroscope, a cable is inserted into a patient's gastrointestinal (GI) tract to transmit images, is a painful and uncomfortable process for the patients. In addition, due to the lack of advanced technology and limited operating facilities, the patient's GI tract cannot be fully examined.

A wireless capsule endoscope (WCE) has been used for the clinical examination of GI diseases since 2000 [3,4]. A WCE significantly reduces the pain compared to a traditional wired gastroscope and is suitable for the elderly, infirm, and critically ill patients. In terms of examination scope, WCE expands the area of GI tract examination, especially in the small intestine's examination.

Israel's Given Imaging company launched the world's first WCE (M2A) [5]. The WCE is well-suited and widely accepted for clinical examination. Japan [6] and South Korea [7] have also launched similar WCE products and greatly improved the definition of pictures. China's first WCE has been developed by Chongqing Jinshan Technology co., Ltd. [8,9], which highlights China's technology level and research interests in this area globally.

Despite significant growth in technology, traditional WCE relies on intestinal peristalsis and its gravity to move passively in the GI tract, resulting in time-consuming and poor examination results. One of the ways to solve this problem is to achieve active control of the WCE. However, obtaining accurate real-time positioning (position and posture) information of the WCE is one of the most challenging steps.

In one of the previous studies, the authors proposed rotating an external permanent magnet (EPM) to manipulate the synchronous rotation of a magnetic spiral-type WCE [10]. A commercial WCE consists of a magnetic shell on the surface of the WCE, and a thread structure on the surface of the magnetic shell. The magnetic shell on the surface of

* Corresponding author.
E-mail address: a.dwivedi@mmu.ac.uk (A. Krishna Dwivedi).

https://doi.org/10.1016/j.jmmm.2022.169939
Received 25 July 2022; Received in revised form 3 September 2022; Accepted 5 September 2022
Available online 10 September 2022

the WCE and the EPM were both magnetized in the radial direction. The WCE rotated synchronously with the rotational speed of the EPM. The thread structure on the WCE converted the rotating motion into the linear motion of the WCE, thus realizing active control of the WCE by the EPM.

In the mixed magnetic field environment, it is impossible to measure only the magnetic signal generated by the WCE itself, because the EPM will produce strong magnetic interference, which will distort positioning results. Therefore, the most critical problem is to minimize the influence of the EPM's magnetic signal in the mixed magnetic field environment.

In order to solve the positioning problem of active control for use in magnetic spiral-type WCE, a novel positioning method for the WCE is proposed in this work. In this method, the magnetic signals of the EPM and the WCE are detected by an up-down symmetric array of magnetic sensors. The best estimates of the WCE's magnetic signals are separated from the mixed magnetic signals by the adaptive least mean squares (LMS) algorithm. Overall, the WCE's magnetic signal can be obtained from a mixed magnetic field using the adaptive LMS algorithm. Thus, the innovation of the positioning method lies in that it can realize precise positioning of the WCE with the existence of the EPM, which will directly lead to the realization of closed-loop active control of the WCE.

The rest of the paper is organized as follows. Section 2 introduces the overall structure of the magnetic positioning system used in this work. The working principle of the adaptive LMS algorithm in a magnetic positioning system is described in Section 3. In Section 4, the experimental setup and results are introduced. Finally, the discussion is presented in Section 5, and concluding remarks are made in Section 6.

2. Overview of the magnetic positioning system

2.1. Imperative elements of the magnetic positioning system

According to the patient's examination scene, a magnetic positioning system is designed [11–15]. As shown in Fig. 1, an up-down symmetric array of magnetic sensors is used to detect the magnetic field generated by the WCE and the EPM. The EPM is placed in the middle of the two magnetic sensor arrays.

The lower sensor array is mainly used to detect the mixed magnetic field generated by the WCE and the EPM. The collected data is used as the input signal to the main channel of the adaptive LMS algorithm. The upper sensor array is mainly used to collect the EPM's magnetic signal as the reference channel signal of the adaptive LMS algorithm. The collected data of the two sensor arrays are output to the computer through a serial port for data processing. The WCE's magnetic signal is extracted from the mixed magnetic field by the adaptive LMS algorithm. Then, the position and posture information of the WCE is calculated by the magnetic positioning algorithm.

2.2. Hardware design of the magnetic positioning system

The hardware circuit is composed of magnetic sensors array module, CD4067BM data channel selection module, Arduino embedded module, and Personal Computer (PC) data processing module. The block diagram of the circuit design of the magnetic positioning system used in this work is shown in Fig. 2.

The specific working process is as follows: when the magnetic positioning system starts to work, the magnetic signal excited by the magnetic shell on the WCE surface is collected by the magnetic sensor array. The distributed magnetic field intensity is represented by a voltage signal. Then, the CD4067BM is used to input the voltage signal into the

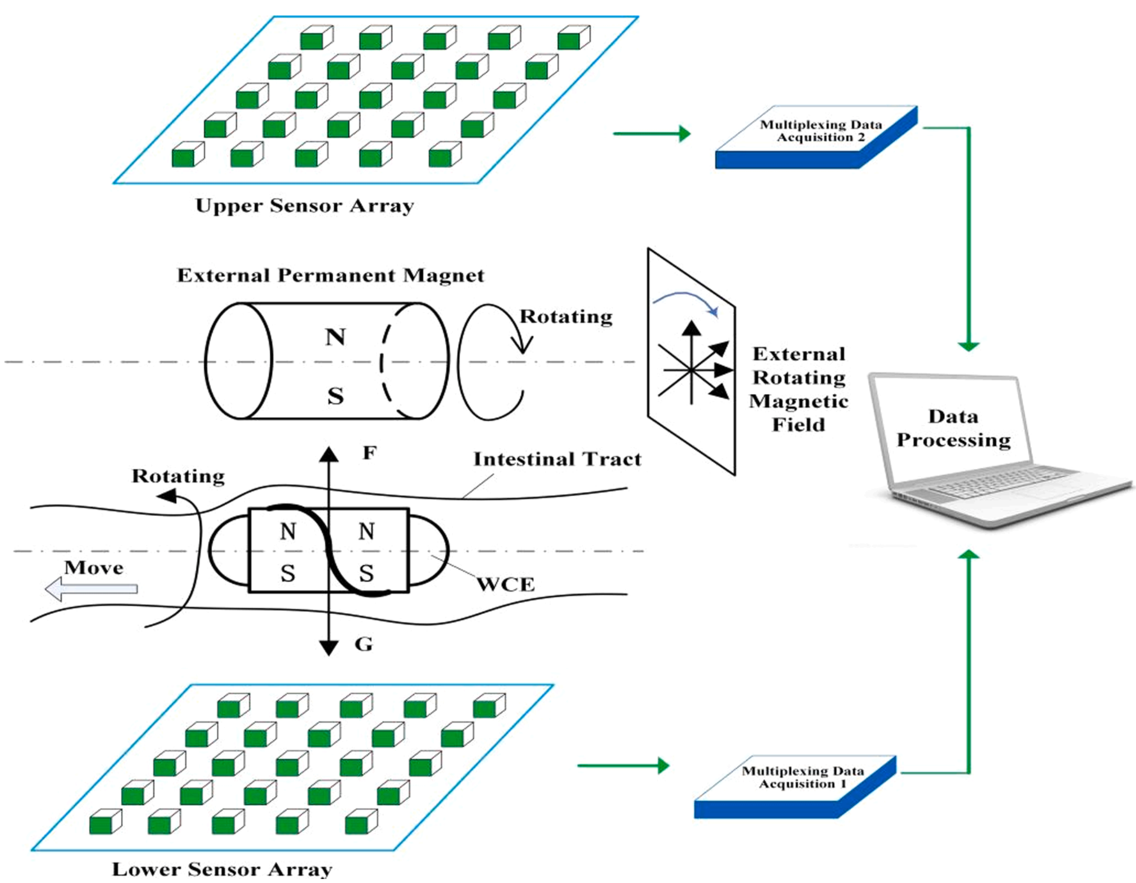

Fig. 1. Positioning system for magnetic active control of magnetic spiral-type WCE.

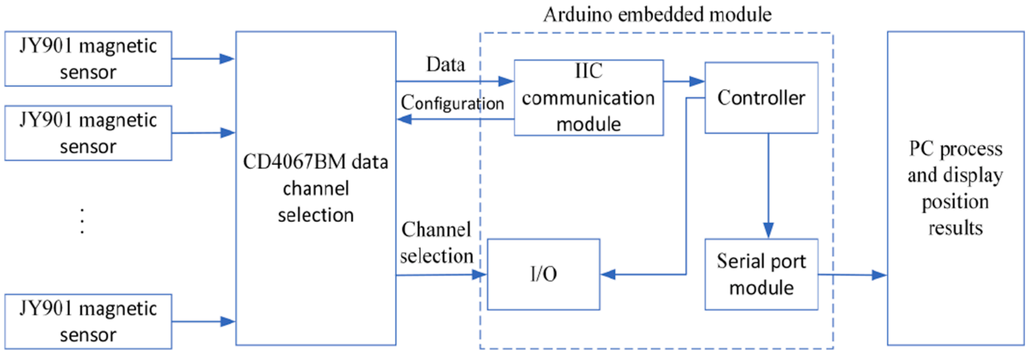

Fig. 2. Block diagram of the circuit design of the magnetic positioning system.

Arduino embedded module in a time-sharing sequence, and the analog to digital (A/D) conversion module in the Arduino samples and filters the analog voltage signal to convert it into a digital voltage signal. At the same time, the channel selection is realized by Arduino controlling the address selection pin of CD4067BM. Finally, the converted digital voltage signal is fed into the PC by the general-purpose input/output (GPIO) port of Arduino through the universal serial bus (USB) to transistor-transistor logic (TTL) module. The PC preprocesses the received data and then calculates the precise position and posture information of the WCE using the positioning algorithm.

2.3. Software design of the magnetic positioning system

2.3.1. Selection of the embedded module

The magnetic positioning system uses the Arduino microcontroller (Arduino Uno R3) as the embedded module. Its standard operating voltage is +5 V. It has 14 digital I/O pins, six of which provide pulse-width modulation (PWM) output and integrates inter-integrated circuit (IIC) modules.

The Arduino is initially configured, before the working of the magnetic positioning system. Then, each magnetic sensor is configured through the IIC interface. At the same time, read and write instructions are sent. The flow chart of the Arduino program design is shown in Fig. 3.

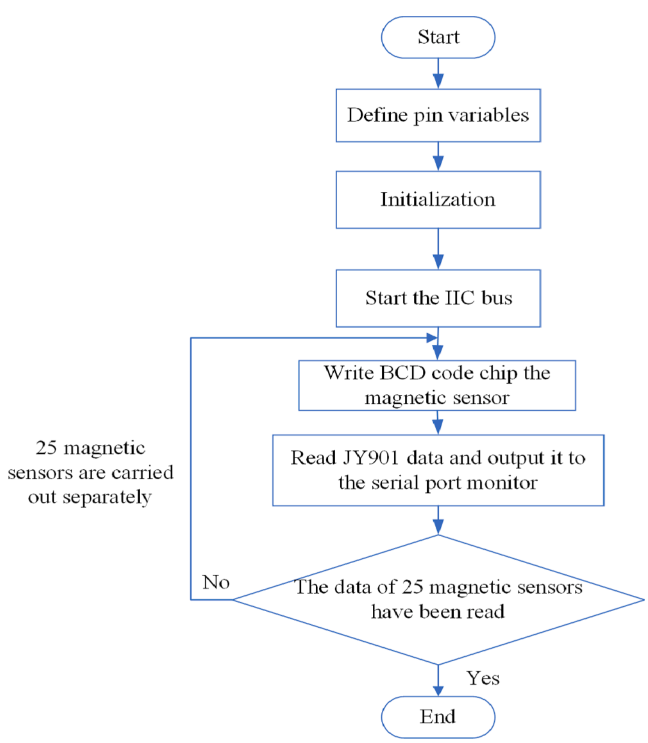

Fig. 3. The flow chart of the program design of Arduino.

2.3.2. Acquisition and preprocessing of magnetic signals

Since strict magnetic shielding cannot be achieved in the experimental environment, the influence of the surrounding magnetic field needs to be considered. The magnetic fields of human tissues can be neglected, hence, the geomagnetic field may be the most significant interference factor in the experiment setup. Moreover, its magnetic field intensity changes relatively steadily. Therefore, the geomagnetic value is collected initially before the experiment. Later, this value is subtracted from the total magnetic field data. Thus, the magnetic field data needed is obtained for the experiment. The flow chart of the steps used for the

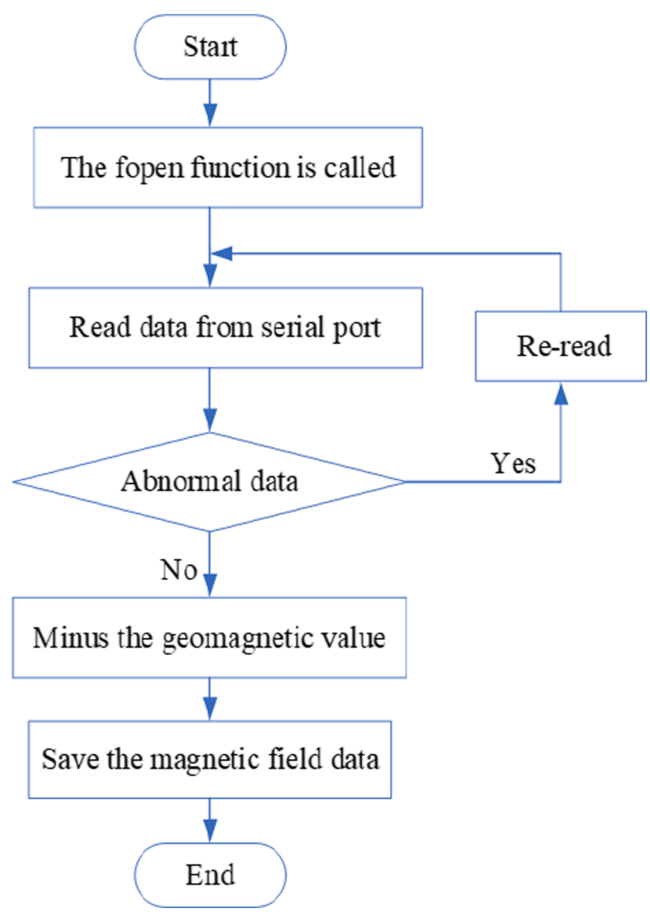

Fig. 4. The flow chart of the steps used for the acquisition and preprocessing of magnetic signals.

acquisition and preprocessing of magnetic signals is shown in Fig. 4.

3. Adaptive noise cancellation of magnetic field

3.1. Principle: Adaptive noise cancellation of magnetic field

The adaptive filter has been developed so far and applied in many aspects. In this experiment, to eliminate magnetic field interference noise, it is used as an adaptive noise canceller [16–19]. However, there are two prerequisites for applying the adaptive filter for noise elimination. Firstly, there must be a strong correlation between the noise in the input signal of the main channel and the reference channel signal. And secondly, the useful signal in the input signal of the main channel does not influence the reference channel signal.

Firstly, the input signal of the main channel is the mixed magnetic signal generated by the WCE and the EPM. The reference channel signal is from the EPM. Therefore, there is a strong correlation between the noise (the EPM's magnetic signal) in the main channel signal and the reference signal. Secondly, the static magnetic field, produced by the magnetic shell on the WCE's surface, has linear attenuation characteristics. When the upper sensor array is a certain height away from the magnetic shell, the magnetic signal of the EPM collected by the upper sensor array is seldom affected by the magnetic shell, which has been verified in later experiments. Therefore, the magnetic positioning system meets the two prerequisites, as stated for applying the adaptive filter for noise elimination.

This paper proposes an adaptive noise cancellation scheme based on the LMS algorithm. It is essential to obtain the best estimation of the WCE's magnetic signals from mixed magnetic fields. The block diagram of the adaptive noise cancellation system of the magnetic field is shown in Fig. 5.

The mixed magnetic signals, generated by the WCE and the EPM, were used as the input signal $d(n)$ of the main channel in the adaptive LMS algorithm. The magnetic signal of the EPM served as the reference channel signal $x(n)$ in the adaptive LMS algorithm. The signal $y(n)$ is obtained by weighting $x(n)$ through the adaptive processor. Then the adaptive LMS algorithm is applied to adjust the weight coefficients of each filter tap. The iterative calculation is carried out so that $y(n)$ is infinitely close to the noise signal $n_1(n)$ in the input signal of the main channel. Finally, through the subtracter, the noise signal $n_1(n)$ present in $d(n)$ is canceled as far as possible to obtain the error signal$e(n)$. When$y(n) = n_1(n)$,$e(n) = s(n)$, the output will be the optimal magnetic signal of the WCE.

3.2. LMS algorithm

The LMS algorithm is easy to calculate and efficient, so it has been widely used in practice. The LMS adaptive algorithm is based on the fastest descent method, which searches along the negative direction of the gradient estimation of the weight in the iterative process and keeps updating the weight coefficient vector to optimize the mean square error [20–23].

As shown in Fig. 5, where the vector of tapping weight coefficient is$w(n) = [w_0(n)\ w_1(n)\ ...\ w_{N-1}(n)]^T$, the reference channel signal is$x(n) = [x(n)\ x(n-1)\ ...\ x(n-N+1)]^T$, and $y(n)$ is the weighted estimation of$x(n)$:

$$y(n) = \sum_{i=0}^{N-1} w_i(n)x(n-i) = \mathbf{w}^T(n)\mathbf{x}(n) \tag{1}$$

The output signal of the noise cancellation system is computed as:

$$e(n) = d(n) - y(n) = d(n) - \mathbf{w}^T(n)\mathbf{x}(n) \tag{2}$$

The square error is computed as:

$$e^2(n) = d^2(n) - 2d(n)\mathbf{x}^T(n)\mathbf{w} + \mathbf{w}^T\mathbf{x}(n)\mathbf{x}^T(n)\mathbf{w} \tag{3}$$

Taking the mathematical expectation on both sides of the above equation to obtain the mean square error:

$$\xi(n) = E[e^2(n)] = E[d^2(n)] - 2\mathbf{P}^T\mathbf{w} + \mathbf{w}^T\mathbf{R}\mathbf{w} \tag{4}$$

$\boldsymbol{P} = E[d(n)\mathbf{x}(n)]$ is the cross-correlation matrix between the input signal of the main channel and the reference channel signal, and $\boldsymbol{R} = E[\mathbf{x}(n)\mathbf{x}^T(n)]$ is the autocorrelation matrix of the reference channel signal.

Eq. (4) takes the partial derivative of the weight coefficient vector **W**. The gradient of the mean square error is computed as:

$$\nabla(n) = \frac{\partial\xi(n)}{\partial w} = \frac{\partial E[e^2(n)]}{\partial w} = 2\boldsymbol{R}\mathbf{w}(n) - 2\boldsymbol{P} \tag{5}$$

Let$\nabla(n) = 0$, and the optimal weight coefficient can be computed as:

$$\boldsymbol{W}_{opt} = \boldsymbol{R}^{-1}\boldsymbol{P} \tag{6}$$

For the sake of simplicity, the fastest descent method is used to approximate the optimal solution.

$$\mathrm{w}(n+1) = \mathrm{w}(n) - \mu\nabla(n) \tag{7}$$

Where, μ is the step size parameter, its value range is$0 < \mu < \frac{1}{\lambda_{\max}}$, and $\lambda_{\max}$ is the maximum eigenvalue of the autocorrelation matrix **R**.

For the calculation of gradient$\boldsymbol{W}$, the square error is directly taken as

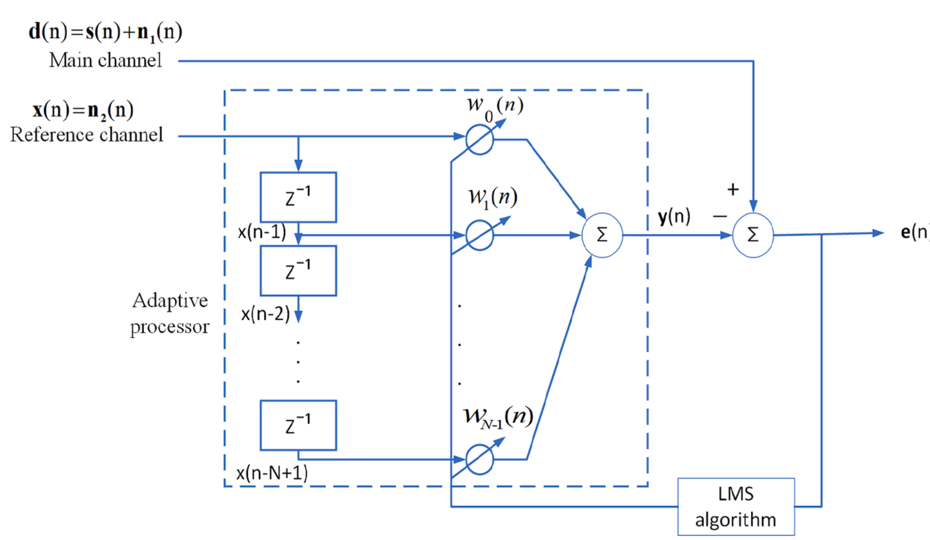

Fig. 5. Block diagram of the adaptive noise cancellation system of the magnetic field.

the estimate of the mean square error.

$$\nabla(n) \approx \widehat{\nabla}(n) = \frac{\partial e^2}{\partial \mathrm{w}} = 2e(n)\frac{\partial e(n)}{\partial \mathrm{w}} = -2e(n)\mathrm{x}(n) \tag{8}$$

Thus, the weight recursive formula of the LMS algorithm can be computed as:

$$\mathrm{w}(n+1) = \mathrm{w}(n) - \mu\nabla(n) = \mathrm{w}(n) + 2\mu e(n)\mathrm{x}(n) \tag{9}$$

When the tap weight vector of the LMS algorithm is close to the optimal value, the EPM's magnetic signal can be filtered as far as possible. Thus, the required magnetic signal of the WCE can be extracted.

3.3. Realization of the adaptive noise cancellation of magnetic field

3.3.1. Selection parameter

In general, the adaptive filter consists of two parts: the filter structure and the adaptive algorithm. The transverse filter structure is used in this experiment because of its good stability and the adaptive algorithm is used to adjust the tap weight coefficient of the filter. The selection of optimal weight coefficient is closely related to filter order, step size, and initial value of the weight vector.

3.3.1.1. The order of the filter. For the selection of filter order, it is necessary to ensure an excellent approximation to the desired signal, as well as to ensure sufficient dynamic characteristics to adapt to the requirements of non-stationary characteristics. Hence, the order selection should be appropriate. Higher-order will lead to slow convergence and cannot meet the effect of real-time processing. Meanwhile, smaller-order will result in poor steady-state performance. In practice, the filter order is first estimated, and then the final order of use is determined by comparing the filtering quality.

3.3.1.2. Step size parameter. The step size parameter adopted in this experiment is the fixed step size parameter. There is no specific formula for selecting its value, but it must meet the value range (as shown in Eq. (7)). If the value is too small, the convergence will be slow; otherwise, the filtering effect will be poor. Because there is strong noise interference in practice, a small initial value in the value range of the step size parameter is selected tentatively. Subsequently, the debugging range of the step size parameter is determined. Then, the initial value is used as a starting point and explored forward according to the debug range. Finally, if the experimental error (as shown in Eq. (11)) decreases, the trial direction is maintained; otherwise, the trial direction is changed and the change in the experimental error is observed until the desired step size parameter is found.

3.3.1.3. The initial value of the weight vector. The data of the reference signal $x(n)$ and the input signal $d(n)$ represent the magnitude and direction of magnetic field intensity. The EPM's magnetic signal has a different influence on each magnetic sensor, which will lead to a negative error signal$e(n)$. If each tap coefficient w_0 is the same, it will cause errors in the experimental results. The initial value of the tap weight vector is set as in Eq. (10), where m is the length of the input signal.

$$w_0 = \begin{cases} 0, & if|d(n)| > |x(n)| \\ 1, & if\ |d(n)| \leqslant |x(n)| \end{cases} \quad (n = 1, 2, ..., m) \tag{10}$$

3.3.2. The implementation process

When the LMS algorithm is used to filter the EPM's magnetic signals, the realization steps are as follows:

1) Set the input signals $d(n)$ of the main channel and the reference channel signal$x(n)$; initialize the filter parameters: order *N,* initial value of the weight vectorw_0, step size parameterμ; and set the number of iterations as the number of sampling values *M* of input data.
2) To perform the iterative weight operation, let$y(n) = \boldsymbol{w}^T(n)\boldsymbol{x}(n)$.
3) Calculating the error signal$e(n) = d(n) - y(n)$.
4) Adjusting the weight vector$\boldsymbol{w}(n+1) = \boldsymbol{w}(n) + 2\mu e(n)\boldsymbol{x}(n)$.
5) To judge whether the LMS algorithm convergence. If the criteria are met, the operation is terminated. Otherwise, when *n* increases by 1, it jumps to steps 2) and 3) for recalculation until the LMS algorithm converges.

The flow chart of the realization of the LMS algorithm is shown in Fig. 6.

3.4. Evaluation index of experimental results

The relative error of results was defined as:

$$\varepsilon = \frac{\bar{e}}{\bar{s}} - 1 \tag{11}$$

$\bar{e}$ is the mean value of $e(n)$ of the WCE's magnetic signal when the LMS algorithm converges and $\bar{s}$ is the mean value of $s(n)$ of the WCE's magnetic signal measured independently. As can be seen from the definition, when ε approaches 0, the magnetic signal of the WCE obtained is closer to the actual measured value.

4. Experiments and result analysis

4.1. Experiments for the system performance test

4.1.1. Measurement range of magnetic sensor

The JY901 magnetic sensor has a specific measurement range, and the magnetic shell on the surface of the WCE has a linear demagnetization characteristic. Therefore, the measurement range of the magnetic sensor must be determined.

In the experiments, firstly, the three-dimensional space coordinates

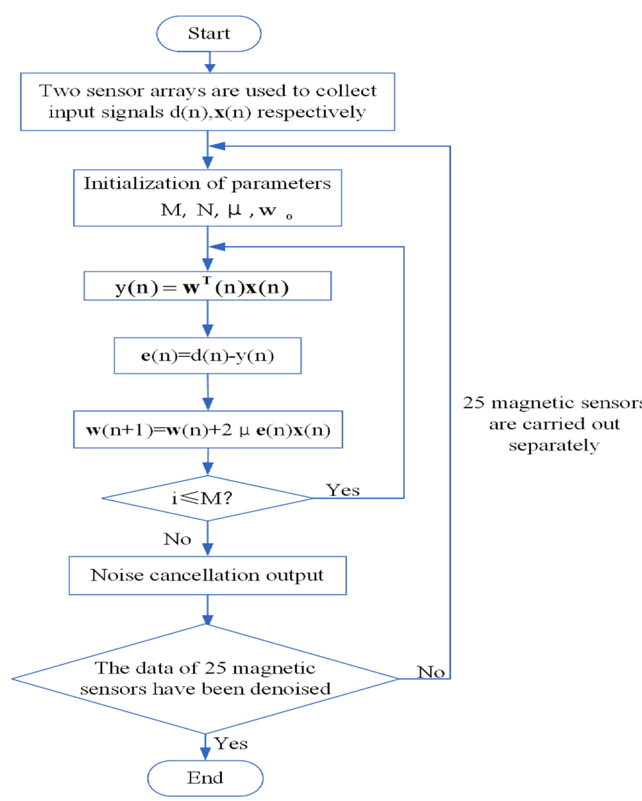

Fig. 6. The flow chart of the realization of the LMS algorithm.

of the magnetic positioning system were established according to the known three-axis direction of JY901. The reference coordinates were set on the coordinate paper plane, and the center point of the coordinate paper was taken as the coordinate origin of the positioning system, as shown in Fig. 7. In order to maintain the acrylic plate flat during the experiments, a three-axis gyroscope was used for calibration. Subsequently, when the data output from the serial port monitor was standard, the radial magnetized magnetic shell was placed directly above the center of the magnetic sensor array. Its magnetic field direction and z-axis of the space coordinate system overlapped, and the space coordinate was (0,0, Z). Finally, the magnetic shell was moved along the Z-axis to observe the changes in data through the serial port monitor. When 4096 (abnormal data value) appeared in the data displayed by the serial port monitor, it indicated that a data overflow occurred, which corresponded to the minimum measured distance. When there was no significant change in data, it corresponded to the maximum measured distance. By this experimental method, the measurement range of the magnetic sensor was 125 mm to 240 mm.

4.1.2. *Test experiments for the reference channel*

In the positioning experiments without magnetic interference, to preset any of the magnetic shell's posture in space and to determine the actual position of the magnetic shell, a three-dimensional position and posture control device is designed as the bracket of the magnetic shell, as shown in Fig. 8. The control device is a plastic bracket with a 360° rotation function so that the magnetic shell can make an arbitrary posture adjustment. The magnetic shell is fixed in the middle position of the wooden pole with the same size as its inner diameter. The perpendicularity and smoothness of the wooden pole have achieved the best performance after processing. Fig. 9 shows the physical design of the magnetic shell used in this work.

According to the preconditions of adaptive filtering, the reference channel signal cannot contain the useful signal in the input signal of the main channel. In this experiment, the upper sensor array is used to detect the EPM's magnetic signal as the reference channel signal, so it should be verified that it does not contain the useful signal (the magnetic shell's magnetic signal) of the main channel.

The experimental platform for magnetic positioning and its sections were set up as shown in Figs. 10 and 11, respectively. The dotted lines represent the boundary of the N and S poles of the EPM and the magnetic shell. Since the EPM controlled the magnetic shell from 108.29 mm to 356.36 mm, to ensure the best synchronous rotation between the two, the control height was set at 250 mm. In addition, in the experiment of exploring the measuring range of the magnetic sensor, the selection range of the magnetic shell's measuring distance (125 mm–240 mm) was determined, so the measuring height of the magnetic shell was set at 186 mm. These values used in the experimental setup were helpful in achieving stable magnetic signals.

After setting up the experimental platform, the upper sensor array was used to test the mixed magnetic signals (the magnetic shell and the EPM), as well as the magnetic signals of the EPM. The measured magnetic field data is shown in Fig. 12. From Fig. 12, it can be observed that in the experiments performed using the estimated height of the magnetic shell, the reference channel signal is not disturbed by the magnetic signal of the magnetic shell.

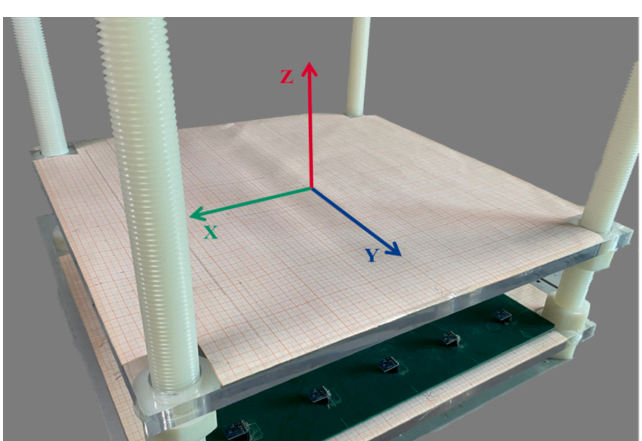

Fig. 7. The experimental setup to estimate the reference coordinates of the magnetic positioning system.

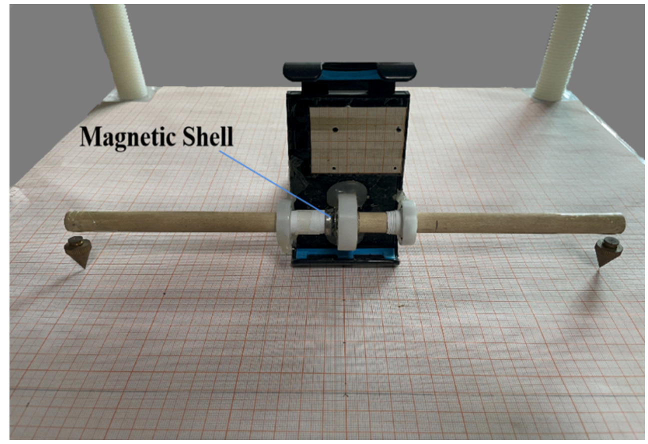

Fig. 8. The control device for the magnetic shell.

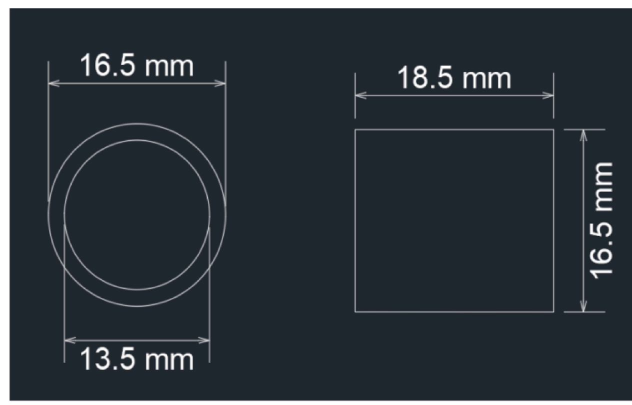

(a) The dimension reference system of the magnetic shell.

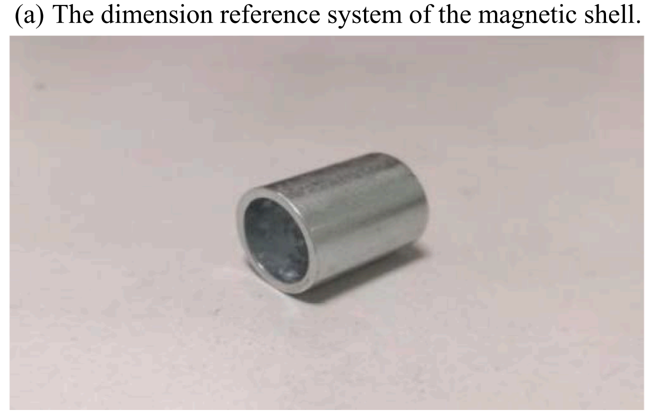

(b) The physical picture of the magnetic shell.

Fig. 9. The physical design of the magnetic shell used in the experiments.

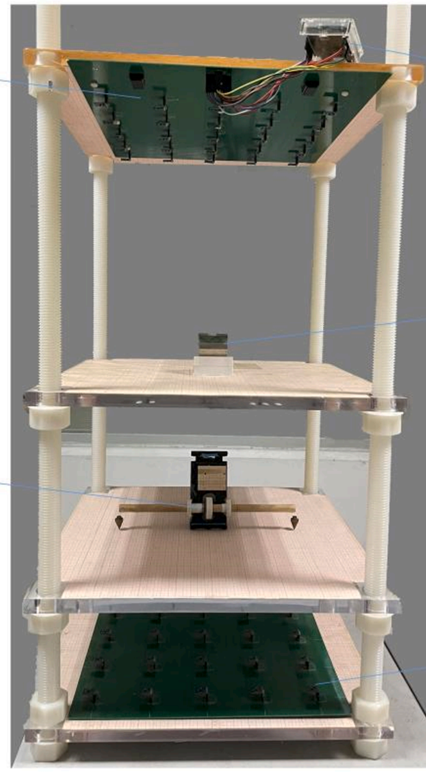

Fig. 10. The experimental setup for the magnetic positioning system.

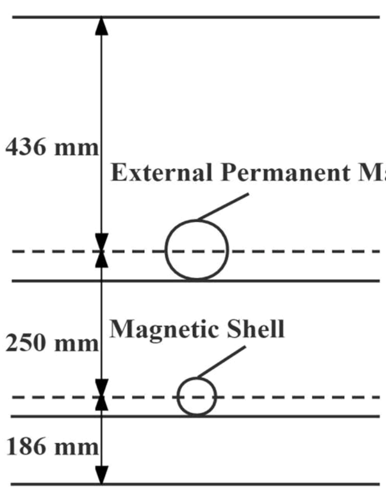

Fig. 11. The section of the experimental setup for the magnetic positioning system.

4.2. *The experimental setup for the adaptive noise cancellation of magnetic field*

4.2.1. *Determination of iteration number*

To improve the accuracy of the experiments, the X, Y, and Z-axis measuring data of the central magnetic sensor were considered for testing. The final iteration number was determined by comparing the relative errors after different iterations.

Firstly, the experimental platform was set up, as shown in Fig. 10. The EPM and the magnetic shell were placed at the central origin of each layer of the coordinate paper. Their magnetic field direction and Z-axis of the space coordinate system overlapped. Then, the data of the upper and lower sensor arrays were collected as the reference channel signal and the main channel signal. Finally, the obtained X, Y, and Z-axis data were processed by the LMS algorithm, and the iteration number was changed to compare the relative error of the results achieved, as shown in Fig. 13.

It can be observed from the data shown in Fig. 13 that the relative error is minimized after 500 or more iterations. However, from the perspective of running time, selecting 500 iterations is more in line with real-time performance.

4.2.2. *Comparison between the measured values and actual values of the magnetic shell's magnetic signal*

For these measurements, the experimental setup, discussed in Section 4.2.1, was used. The adaptive LMS algorithm was applied to the filter setup and the number of iterations was set to 500. Finally, the three-axis components of the magnetic shell's magnetic signal and the corresponding relative errors were computed. The measured values are shown in Figs. 14 and 15, respectively.

As seen from the variation trend in Fig. 14, the magnetic shell's magnetic signal extracted from the mixed magnetic field is close to its actual signal. Additionally, according to Fig. 15, the average relative error ofB_x,B_y, and B_z is 2.04 %, 2.20 %, and 1.47 %, respectively. The total average relative error is 1.90 %. The achieved results show that the overall effect of the experiments is good, and the best measurement value of the magnetic shell's magnetic signal can be obtained.

4.3. *Error analysis and future work*

Although the experimental setup helped in achieving the intended aims of this work, there are still a few areas where the performance can be improved. For instance, it was challenging to ensure the stability of

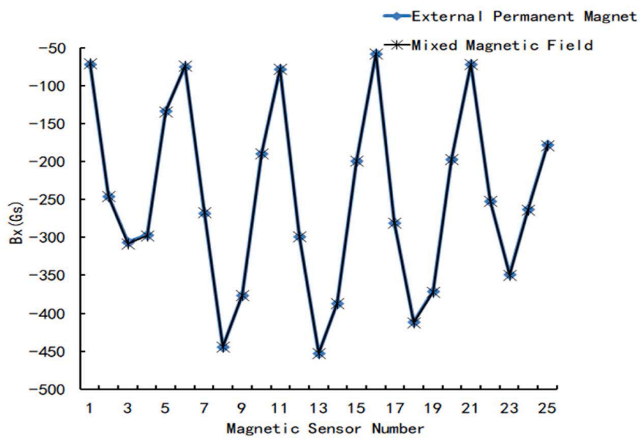

(a) Data comparison in the X-axis direction.

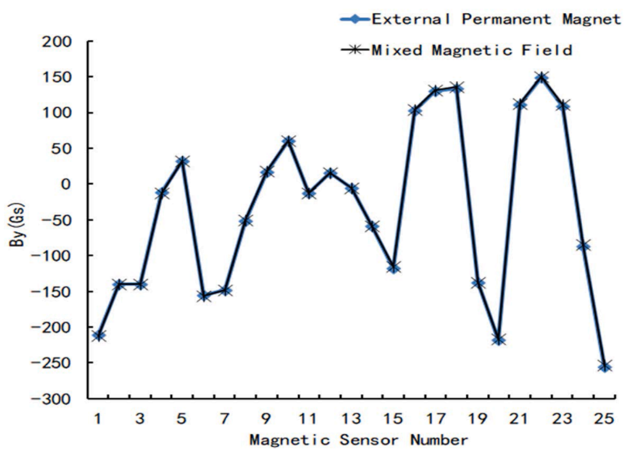

(b) Data comparison in the Y-axis direction.

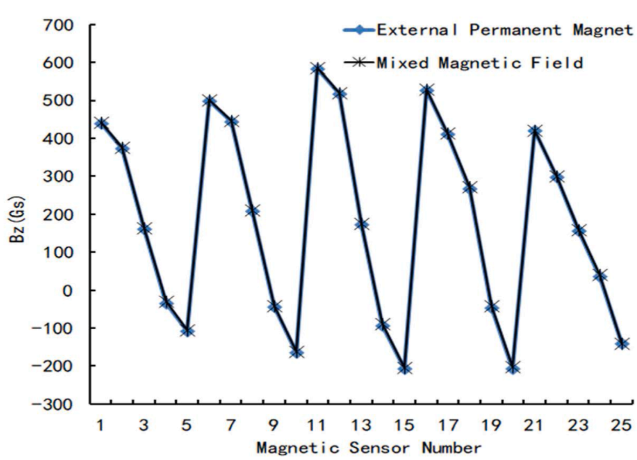

(c) Data comparison in the Z-axis direction.

Fig. 12. Comparison of experimental data of the reference channel for the three axes.

the WCE's magnetic signal acquired by the magnetic positioning system. Additionally, the calibration accuracy of each sensor was different, resulting in different stability. Furthermore, there were some errors between the actual values and the measured values due to the variation of the magnetic field due to the external environment. These experiments were carried out without obvious environmental magnetic interference. However, the conditions in medical applications will be more complicated. Therefore, in future work, it is necessary to analyze

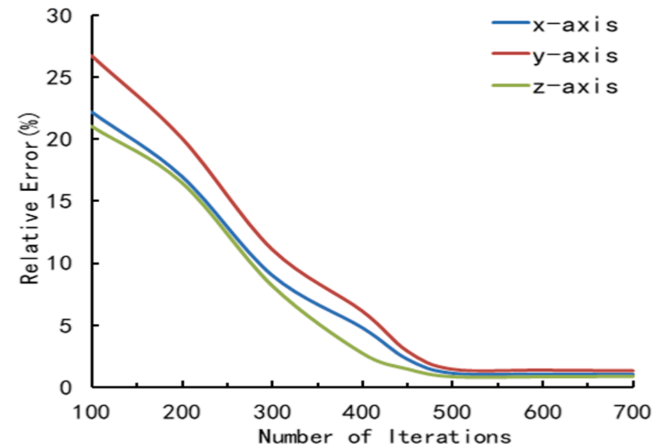

Fig. 13. The relative error of triaxial experimental data varies with the number of iterations.

the positioning experiments under complicated conditions.

5. Discussions

In order to apply the proposed WCE positioning method for the clinical application, further consideration should be given to the positioning algorithm processing of filtered data. For instance, to obtain more accurate positioning information, the authors are researching the establishment of multiple equations based on the magnetic dipole model, and solving the unknown parameters through linear or nonlinear algorithms.

The biggest advantage of the method is that it can achieve the precise positioning of the WCE in an environment with strong magnetic interference. This will be applied in future work to maintain active control of the WCE by the EPM. Therefore, the method will drive the realization of closed-loop control of the WCE, which has great potential in future clinical applications.

6. Conclusion

In this research, the effectiveness and feasibility of applying the adaptive LMS algorithm in WCE of active control were verified by experiments. In order to eliminate the strong magnetic interference caused by the EPM, the authors proposed a new positioning method of WCE. Based on the principle of adaptive noise cancellation of the magnetic field, the magnetic positioning model was established. The cancellation effect of magnetic signals under different iterations and the final relative error of triaxial magnetic signals were measured. After magnetic signal cancellation by using the adaptive LMS algorithm, the average relative error of the WCE's triaxial magnetic signals was found to be 2.04 %, 2.20 %, and 1.47 % respectively, and the total average relative error was 1.90 %. The experimental results show that satisfactory results were achieved using the methods discussed, and the WCE's magnetic signal can be extracted from the mixed magnetic field as required for clinical applications. This will promote the realization of closed-loop control of the WCE, which has significant medical value and deserves further research.

CRediT authorship contribution statement

Bo Ye: Writing – original draft, Investigation, Methodology, Writing – review & editing. **Guo Fang:** Writing – original draft, Investigation, Methodology. **Jinping Hu:** Data curation, Formal analysis. **Hao Wang:** Software, Methodology. **Yingbing Fu:** Software, Validation. **Shicong Zhang:** Resources, Visualization. **Amit Krishna Dwivedi:** Project administration, Supervision, Writing – review & editing.

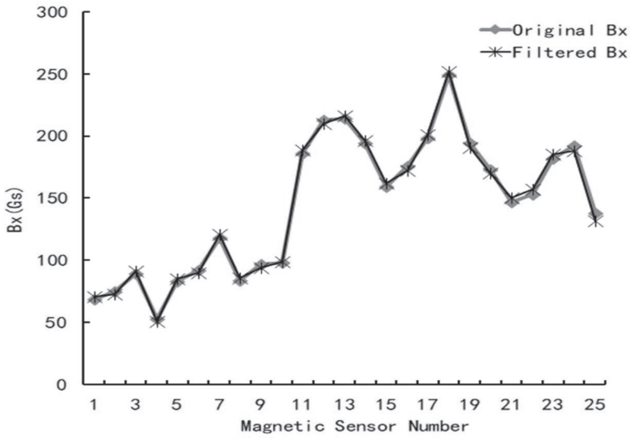

(a) Data comparison in the X-axis direction.

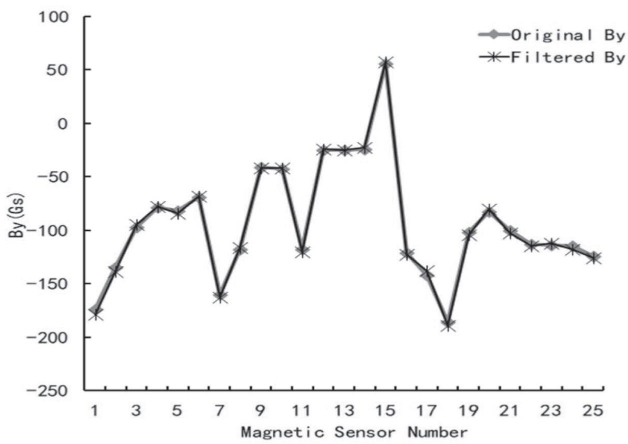

(b) Data comparison in the Y-axis direction.

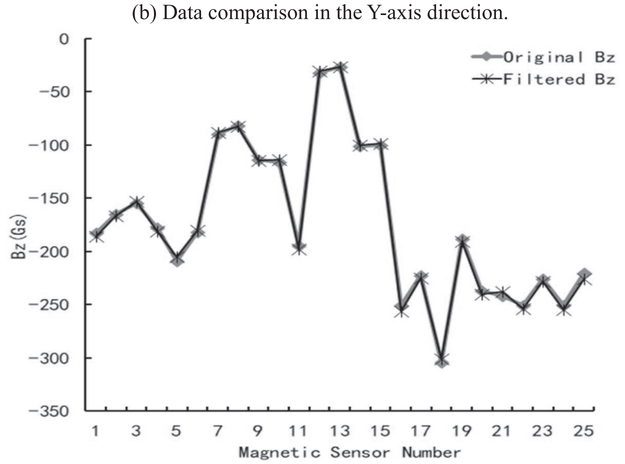

(c) Data comparison in the Z-axis direction.

Fig. 14. Comparison of the measured values and actual values of magnetic shell's magnetic signal.

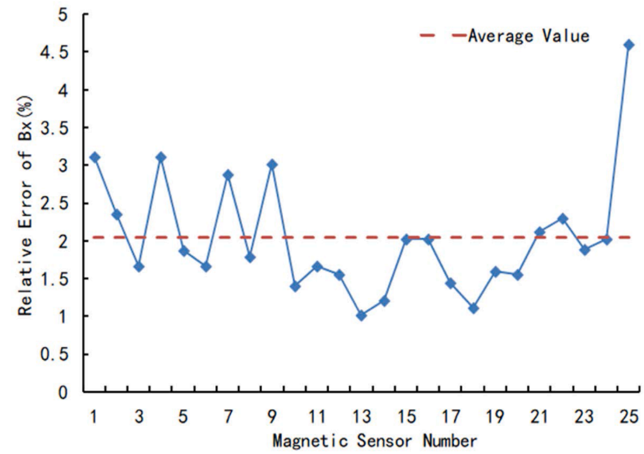

(a) The relative error in the X-axis direction.

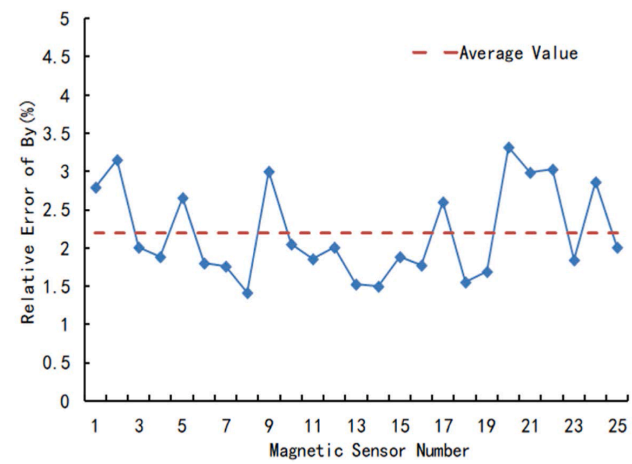

(b) The relative error in the Y-axis direction.

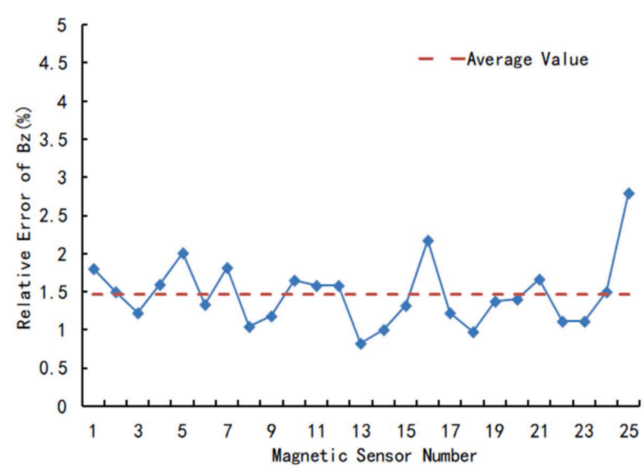

(c) The relative error in the Z-axis direction.

Fig. 15. The relative error in the measured values.

Declaration of Competing Interest

The authors declare that they have no known competing financial interests or personal relationships that could have appeared to influence the work reported in this paper.

Data availability

No data was used for the research described in the article.

Acknowledgments

The authors would like to thank Mr. W. Zha and Miss. J. Chen for their help in conducting the experiments.

References

[1] M. Zhang, X.J. Yang, Effects of a high fat diet on intestinal microbiota and gastrointestinal diseases, World J. Gastroenterol. 22 (40) (2016) 8905.
[2] G.L. Trakman, S. Fehily, C. Basnayake, A.L. Hamilton, E. Russell, A. Wilson-O'Brien, M.A. Kamm, Diet and gut microbiome in gastrointestinal disease, J. Gastroenterol. Hepatol. 37 (2) (2022) 237–245.
[3] G. Iddan, G. Meron, A. Glukhovsky, P. Swain, Wireless capsule endoscopy, Nature 405 (6785) (2000) 417.
[4] G.J. Iddan, C.P. Swain, History and development of capsule endoscopy, Gastroint. Endoscopy Clin. 14 (1) (2004) 1–9.
[5] G. Pan, G. Yan, X. Qiu, J. Cui, Bleeding detection in wireless capsule endoscopy based on probabilistic neural network, J. Med. Syst. 35 (6) (2011) 1477–1484.
[6] J.F. Rey, The future of capsule endoscopy, Keio J. Med. 62 (2) (2013) 41–46.
[7] G. Pan, L. Wang, Swallowable wireless capsule endoscopy: progress and technical challenges, Gastroenterol. Res. Pract. 2012 (2012) 1–9.
[8] N. Hosoe, K. Takabayashi, H. Ogata, T. Kanai, Capsule endoscopy for small-intestinal disorders: current status, Dig. Endosc. 31 (5) (2019) 498–507.
[9] L. Zhang, J. Shen, L. Guo, F. Cheng, Q.i. Fan, K. Ni, S. Xia, D. Zhou, Diagnostic value of OMOM capsule endoscopy for small bowel diseases in adults, Exp. Ther. Med. (2018).
[10] Bo. Ye, W. Zhang, Z.-J. Sun, L. Guo, C. Deng, Y.-q. Chen, H.-h. Zhang, S. Liu, Study on a magnetic spiral-type wireless capsule endoscope controlled by rotational external permanent magnet, J. Magn. Magn. Mater. 395 (2015) 316–323.
[11] H. Mateen, R. Basar, A.U. Ahmed, M.Y. Ahmad, Localization of wireless capsule endoscope: a systematic review, IEEE Sens. J. 17 (5) (2017) 1197–1206.
[12] S. Song, S. Wang, S. Yuan, J. Wang, W. Liu, M.-H. Meng, Magnetic tracking of wireless capsule endoscope in mobile setup based on differential signals, IEEE Trans. Instrum. Meas. 70 (2021) 1–8.
[13] Y. Xu, M.Q.H. Meng, Free sensor array based relative localization system for wireless capsule endoscopy, in: 2018 IEEE International Conference on Robotics and Biomimetics (ROBIO), 2018, pp. 550–555.
[14] N. Dey, A.S. Ashour, F. Shi, R.S. Sherratt, Wireless capsule gastrointestinal endoscopy: direction-of-arrival estimation based localization survey, IEEE Rev. Biomed. Eng. 10 (2017) 2–11.
[15] S.-Y. Yen, H.-E. Huang, H.-C. Chen, F.-W. Huang, F.-M. Suk, G.-S. Lien, C.-W. Liu, A novel method for locating a magnetic-assisted capsule endoscope system, IEEE Trans. Magn. 56 (10) (2020) 1–6.
[16] Least-mean-Square Adaptive Filters, John Wiley & Sons; 2003.
[17] A. Dickman, Adaptive Filters Adaptive filters[M]//Verified Signal Processing Algorithms in Matlab and C: Advised by Israel Greiss, Springer International Publishing, Cham, 2022, pp. 145–159.
[18] F. Jin, S. Cao, Automotive radar interference mitigation using adaptive noise canceller, IEEE Trans. Veh. Technol. 68 (4) (2019) 3747–3754.
[19] C. Chi, V. Pallayil, M. Chitre, Design of an adaptive noise canceller for improving performance of an autonomous underwater vehicle-towed linear array, Ocean Eng. 202 (2020) 106886.
[20] D. Cao, Z. Chen, X. Gao, Research on noise reduction algorithm based on combination of LMS filter and spectral subtraction, J. Inf. Process. Syst. 15 (4) (2019) 748–764.
[21] L. Gan, H. Zhang, Variable step least mean square adaptive filtering method for wireless capsule endoscopy positioning system, Optik 171 (2018) 543–551.
[22] I. Jubran, A. Maalouf, D. Feldman, Fast and accurate least-mean-squares solvers, 2019.
[23] A.D. Poularikas, Adaptive Filtering: Fundamentals of Least Mean Squares with MATLAB®, CRC Press, 2017.